Enhanced resolution ERS-1 scatterometer imaging with irregular samples

D. G. Long and D. S. Early

Brigham Young University, Electrical and Computer Engineering Dept.
Provo, Utah 84602 USA

ABSTRACT

Scatterometers are low (25-50 km) resolution radars originally designed to measure winds over the ocean from space. They measure the normalized radar backscatter coefficient (σ^o) from which the wind is estimated. Over land and ice σ^o is very sensitive to surface conditions and is useful for various scientific studies. Unfortunately, the low resolution of the measurements limits the application of the data. The Scatterometer Image Reconstruction (SIR) algorithm can produce significantly enhanced resolution radar images by taking advantage of measurement overlap from multiple passes of the radar over the target site. The resulting measurements are on an irregular grid and may have different response functions making the analysis of the non-linear SIR algorithm very complicated. Analysis of SIR is further complicated by the fact that it is bivariate: two separate but related images ($\mathcal{A}$ and $\mathcal{B}$) are determined from the σ^o measurements where σ^o is related to $\mathcal{A}$ and $\mathcal{B}$ by the expression $\sigma^o = \mathcal{A} + \mathcal{B}(\theta - 40°)$ where θ is the incidence angle of the measurement which varies from measurement to measurement.

In this paper we provide a theoretical framework for scatterometer image reconstruction and resolution enhancement on irregular grids and provide examples of the resolution enhancement possible for the ERS-1 AMI scatterometer. The paper should be of interest to other researchers dealing with resolution enhancement on irregular grids.

Keywords: scatterometry, ERS-1, resolution enhancement, irregular sampling

1. INTRODUCTION

Studies of the Earth's surface are currently being carried out using a wide variety of instruments and platforms. Space-based platforms offer the most comprehensive spatial and temporal coverage, although the resolution is much less than systems flown on airplanes or surface-based systems. The work presented herein is directed towards developing a compromise between the high resolution of synthetic aperture radar (SAR) and the frequent, wide-area coverage of lower resolution sensors such as scatterometers by developing signal processing techniques to use traditionally low resolution platforms in innovative ways.[5,11]

In this paper, we discuss a theory for resolution enhancement from irregular samples and apply it for scatterometer resolution enhancement. While the theory and techniques are illustrated for enhanced resolution ERS-1 scatterometer imagery, they are generally applicable. The paper is divided into four main sections. In the first, a measurement model is presented. Second, a theory of image reconstruction from irregular samples is presented. In the third section, we demonstrate that reconstruction can recover sidelobe information and we consider the practical use of the theory with the addition of noise to the reconstruction. We discuss scatterometer image reconstruction (SIR), a derivative of multiplicative ART tailored to reduce the influence of noise on enhanced resolution image reconstruction from scatterometer data.[11] Finally, we demonstrate the SIR algorithm for ERS-1 scatterometer resolution enhancement.

Other author information: (Send correspondence to: D.G.L.)
D.G.L.: Email: long@ee.byu.edu; Telephone: 801-378-4383; Fax: 801-378-6586
D.S.E.: earlyd@ee.byu.edu

SPIE Vol. 3170 • 0277-786X/97/$10.00

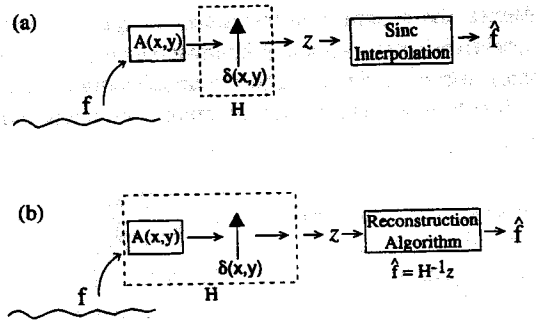

Figure 1. Block diagram illustrating sampling and signal recovery. The original surface, f, is filtered by the system aperture function, $A(x, y)$, and sampled to obtain the measurements z. In (a), the signal is uniformly sampled. The surface function is recovered using low pass filtering which inverts only the sampling. In (b), the operator inverted, denoted by H and the dotted box, includes both the aperture function and the sampling. Sampling is dense and may be irregular.

2. SYSTEM MODEL

While the theory discussed here centers around a model of the surface response that describes the microwave backscatter from a point, it is generally applicable. We desire to make images of the backscatter from ERS-1 scatterometer[1] measurements. We model the radar backscatter (σ^o) from the surface as a function of location with (for the moment) the backscatter's incidence angle dependence suppressed.

Let $f(x, y)$ be the function that gives the backscatter from a point (x, y) on the surface. The measurement system can be modeled by

$$z = Hf + \text{noise} \tag{1}$$

where H is an operator that models the measurement system (aperture filtering and sample spacing), f is the true surface function, and z represents measurements of σ^o made by the instrument. For resolution enhancement, we are interested in the inverse problem:

$$\hat{f} = \hat{H}^{-1}z \tag{2}$$

where $\hat{f}$ is an estimate of f from the measurements z. The inverse of the operator H, $\hat{H}^{-1}$, is exact only if the measurements are noise free and H is invertible, in which case $\hat{f} = f$.

Real-life sampling usually involves a non-ideal sampler with a finite aperture which low-pass filters the data. The aperture functions may have frequency nulls that result in information which can not be recovered. However if suitably sampled and processed, information in the aperture frequency response sidelobes can be recovered if the signal-to-noise ratio (SNR) is sufficiently high.

The traditional approach to sampling and reconstruction is based on the Nyquist sampling theorem which states that a band limited function can be completely reconstructed from regularly spaced samples if the sample rate exceeds the Nyquist sample rate of twice the maximum frequency in the signal. The reconstruction is done with a simple low pass filter consistent with the sampling. The filter is equivalent to using a *sinc* function as an interpolating function (see Fig. 1). When possible, the aperture function is designed to act as a prefilter to eliminate high frequency components of the signal that might otherwise cause aliasing in the reconstructed signal. Such an approach was used with the ERS-1 scatterometer design: A desired sample spacing of 25 km dictated an aperture function that filters wavelengths smaller than 50 km to minimize aliasing.

Because the aperture function is non-ideal, if the data is over-sampled at least some of the higher frequency content of the original signal can be recovered using a reconstruction algorithm which inverts both the sampling and aperture functions [see Fig. 1(b)].

Figure 2 presents a chart comparing the two methods outlined above. Each row of the chart represents the spectra of (from top to bottom) the original image function, the aperture function and the reconstructed estimate of

the function. The dotted lines represents the recoverable frequency range based on sample spacing. In the column 'Traditional Sampling' the dotted lines are narrowly spaced because the sample spacing is larger, and the aperture function and the low pass reconstruction filter are designed to reduce aliasing by attenuating higher frequencies. The 'Reconstruction' column shows the dotted lines spaced further apart because the reconstructed frequency range is increased by more dense sampling.

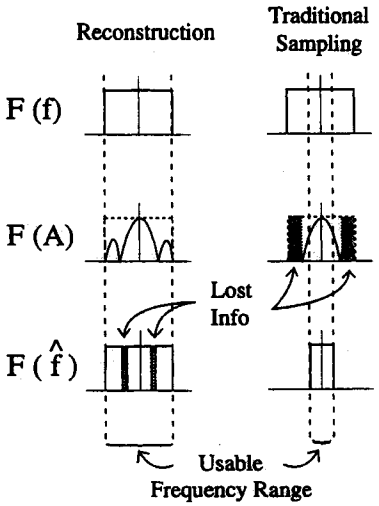

Figure 2. A comparison of the spectrum at various stages of the signal recovery problem illustrated in Figure 1. The rows of the chart represent the spectra of (top to bottom) the original signal, the aperture function and the reconstructed estimate of the signal. The dotted lines show the frequency range recoverable based on the sample spacing. In "Reconstruction," close (but possibly irregular) sample spacing is used with the estimate limited by the nulls in the aperture function frequency response. In "Traditional Sampling," the recoverable range is limited to the Nyquist frequency corresponding to the uniform sample spacing which corresponds to the twice the frequency of the main lobe of the aperture function's frequency response.

3. IRREGULAR SAMPLING AND RECONSTRUCTION THEORY

In this section we consider irregular sampling and reconstruction. We are interested in irregular sampling because we can combine multiple passes of a scatterometer to achieve a closely spaced irregular sample grid.[7]

First, we establish some terminology. Let $L^2(R)$ denote the Hilbert Space of square-integrable functions on R^2 with the norm $\|f\| = (\int_{-\infty}^{\infty} |f(x)|^2\, dx)^{\frac{1}{2}}$. Let $\Omega \subseteq R^2$ be a compact set where Ω denotes the cube $\prod_{i=1}^{2}[-\omega_i, \omega_i]$. The $\omega = (\omega_1, \omega_2)$ define the **extension** of Ω. Finally, let $B^2(\Omega)$ be a closed subset of $L^2(R)$ such that $B^2(\Omega) = \{f \in L^2(R) : supp\, F \subseteq \Omega\}$ where F is the Fourier Transform of f. $B^2(\Omega)$ is, by definition, a Banach space. These three definitions provide a mathematical formalism for the discussion to follow.

Next are two definitions that are used to describe an operator used in the reconstruction algorithm to be presented later. First, an operator A is bounded on the space B if there exists a constant C such that

$$\|Au\| \leq C\|u\| \quad \forall u \in B.$$

Second, the operator norm, denoted $\|\cdot\|'$ is the smallest constant C such that

$$\|A\|' = sup_{\|u\|=1}\|Au\|.$$

Now consider the irregular sampling grid which can b described as δ-dense for the 1-D and 2-D cases as follows[2]: A sampling sequence $X = (x_i)_{i\in Z}, \ldots < x_{i-1} < x_i < x_{i+1} < \ldots$, is said to be δ-*dense* if $sup_i(x_{i+1} - x_i) \leq \delta$. A sampling sequence $X = (x_i)_{i\in Z}$ in R^2 ($x_i = (\xi_1, \xi_2)$) is $\delta = (\delta_1, \delta_2)$-*dense* if $\bigcup_{i\in Z} B_\delta(x_i) = R^2$ where $B_\delta(x_i)$ represents the square $\prod_{i=1}^{2}[\xi_i - \frac{\delta_i}{2}, \xi_i + \frac{\delta_i}{2}]$ centered at x_i.

The 1-D case is presented for use as background to the more applicable 2-D case, but in this treatment, any reference to δ-dense is to the 2-D case unless otherwise specified. In the 1-D case, δ is determined by the largest separation between two sample points. For an intuitive insight, consider a 1-D case and recall that the reconstruction from regular samples is an interpolation using the $sinc(x)$ as an interpolation function. If the samples are not close enough together, the interpolation function cannot reconstruct the signal properly between samples.

For the 2-D case δ-dense is defined as the minimum value of δ around each sample point that completely fills the R^2 space. In Fig. 3(a), a set of sample points is shown with a δ_1 box surrounding each sample point. Note that the union of the boxes is not sufficient to cover the entire R^2 space. In Fig. 3(b), a larger δ value, δ_2, is used that does cover the entire space. Thus, this particular sampling set is δ-Dense with $\delta = (\delta_2, \delta_2)$. In reality, since a sampling set is limited to some finite space in R^2, we assume that the sampling set is periodic in space with a period determined by the x and y dimension of the finite sample space. By extension, the entire R^2 space is then covered by the union of the δ_2 boxes for the periodic grid.

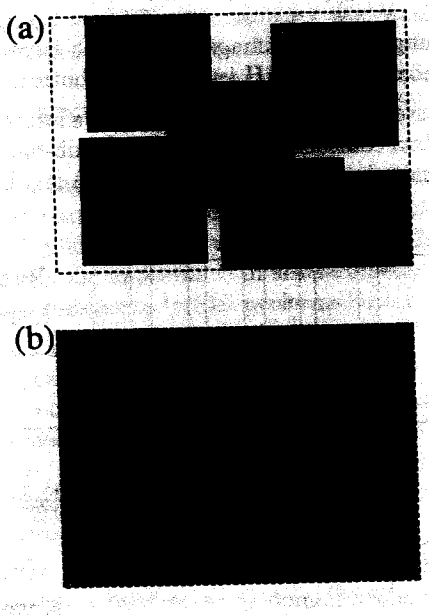

Figure 3. A graphical illustration of δ-dense in 2-D. (a) δ is smaller than the union of the boxes around each sample point to cover the entire R^2 space. (b) A larger δ where the union of the boxes spans the R^2 space. δ-dense corresponds to the smallest δ for which the R^2 space is spanned.

Gröchenig analyzed the reconstruction problem for an irregular sampled surface.[2] He presented a lemma which can be stated as follows: Let A be a bounded operator on a Banach space B such that $\|I - A\|' < 1$ (I is the Identity Operator), where $\|\cdot\|'$ denotes the operator norm on B. Then A is invertible on B and $A^{-1} = \sum_{n=0}^{\infty}(I - A)^n$. Moreover, every $f \in B$ can be reconstructed by the iteration

$$\phi_0 = Af$$
$$\phi_{n+1} = \phi_n - A\phi_n$$
$$f = \sum_{n=0}^{\infty} \phi_n$$

with convergence in B. The operator A which includes the sampling and aperture functions must be bounded with $\|I - A\|' < 1$.

Gröchenig showed that if f is band limited on a Banach space and sampling is δ-dense with $\delta \cdot \omega < ln(2)$ where ω represents the highest frequencies present in f, f can be reconstructed from its samples using this algorithm.[2]

Experimental results for the ERS-1 scatterometer when several days of data are considered show that in the polar regions, the sampling sets are δ-dense with $\delta = 10$ km to 13 km.[7] The best resolution recovery is thus approximately 30 km, a value consistent with experimental results.[7]

It can be shown that Gröchenig's Algorithm is functionally equivalent to the additive algebraic reconstruction technique (ART), a well-established image reconstruction technique.[6] Block additive ART can be written as[3]

$$a_{n+1}^j = a_n^j + \frac{\sum_i (s_i - p_i) h_{ij}}{\sum_i h_{ij}} \tag{3}$$

where a represents the image to be estimated, a_n is the n^{th} iterative estimate of a, j is the pixel index and i is the measurement index. The essence of this equation is that all measurements that touch a pixel a^j are summed and normalized to create the per pixel update value. Eq. (3) can be written as

$$a_{n+1} = a_n + \mathcal{H}(a - a_n) \tag{4}$$

where the a's are now vectors with a being the 'true' image, a_n the nth iterative estimate of a and $\mathcal{H} = H'H$ is an $N \times N$ matrix operator equivalent to Gröchenig's A.[6] H incorporates both the sampling and the aperture function.

While Gröchenig was primarily interested in low-pass function, we are interested in signals sampled by an aperture function with side lobes and nulls. We thus consider the more general sub-band limiting scheme illustrated in Fig.4. It can be shown that such a sub-band limited space defined in Fig. 4(a) is a Banach space.[6]

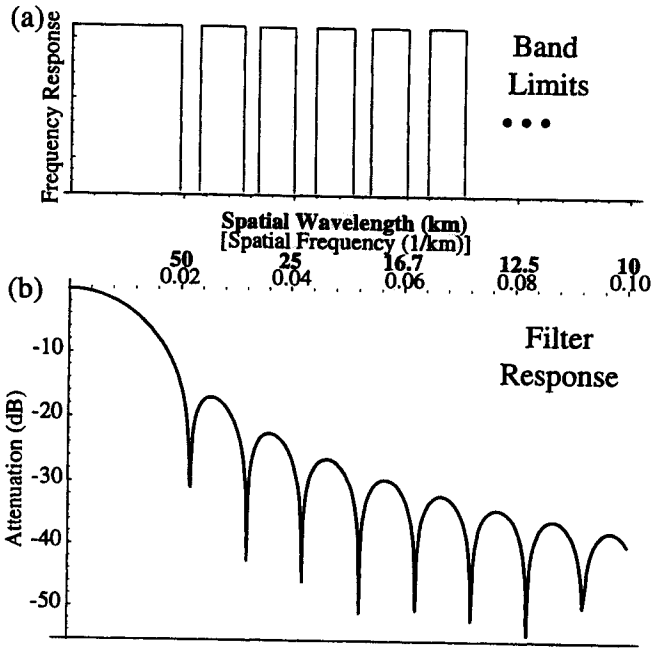

Figure 4. (a) A band limiting scheme that delimits nulls in the filter response in (b). (b) Frequency response of the ERS-1 scatterometer.

In the following discussion we assume that the sample spacing is adequate (δ-dense) for recovering the desired original and deal strictly with aperture function affects on invertiblity. We define the domain of H to be $u \in B^2(\Omega')$ which consists of all functions with a sub-band limited frequency response as illustrated in Figure 4(a). The low pass characteristics of the aperture function built into the operator H indicate that certain frequencies of an arbitrary input are nulled out and therefore unrecoverable in any reconstruction. By setting the domain $B^2(\Omega')$ to be exclusively functions without those frequencies, no information is lost for $v = Hu$, though v may have attenuated frequency components. Then, $u' = H'v = H'Hu \in B^2(\Omega')$ is also in the original Banach space. Thus, $\mathcal{H} = H'H$ is a bounded

operator on the sub-band limited Banach space, meeting the first requirement of Gröchenig's Lemma. Further, $\mathcal{H}$ will be invertible on this Banach space. It follows that Eq. (4) represents a valid algorithm for the *complete* recovery of the original vector a within Banach space $B^2(\Omega')$. Note, however, that *complete* recovery is only possible if the original function is contained in the Banach space spanned by the operator inverse $\mathcal{H}^{-1}$, i.e., $B^2(\Omega')$. Otherwise, as discussed below, the result is an approximation of the original function.

4. PRACTICAL APPLICATION

While $\mathcal{H}$ is a valid operator for Gröchenig's algorithm for function which is band-limited or sub-band-limited, in application the surface function may not be sub-band limited. The original function can only be recovered in the sub-bands over which $\mathcal{H}$ is invertible. Ideally, we would modify or reduce the space to correspond to a band-limited form. However, it is frequently impractical, from an algorithmic and computational standpoint, to reduce the problem to such a form. Instead, for practical application regularization of $\mathcal{H}$ is used to insure its invertiblity over the full space. The ART algorithms implicitly include regularization. Block additive ART is a least squares solution to the inverse problem in Eq. (2) while multiplicative ART with damping is a maximum entropy estimate in the limit.[3,8] A maximum entropy estimate produces a generally "sharper" image than least squares, at least for high contrast images.[9] Maximum entropy can also insure a positive image if desired. Because regularization is used in the ART algorithms, even if the complete original function is unrecoverable, the ART algorithms provide good estimates of the original function.

We now consider the Scatterometer Image Reconstruction (SIR) algorithm. SIR is a modified multiplicative ART algorithm specifically designed for scatterometer data reconstruction to reduce the effects of noise in the reconstruction.[7,10,4,11] SIR is based multiplicative ART with square root damping and includes a non-linearity in the update to minimize the effects of noise. Of importance in scatterometer applications is that SIR also estimates the incidence angle dependence of the measurements.[11] SIR performs better in the presence of noise than the related ART algorithms.

The results of additive ART, multiplicative ART and SIR are similar in the noiseless case. However, because of noise in the measurements, none of the reconstruction algorithms can be run for more than a few dozen iterations so the theoretical limits may not be reached. Nevertheless, as will be shown the algorithms provide good resolution enhancement with only limited iterations. The limited iteration results are *approximations* of the least squares or maximum entropy solution. Experimental results demonstrate that even highly attenuated frequency components are effectively recovered with finite iterations.

In order to illustrate and compare the ART and the SIR algorithm each are applied to a simple 1-D signal. A *sinc* function was chosen since it readily shows the frequency domain reconstruction from the various methods. The test signal is sampled with an irregular sampling grid. A rectangular aperture was chosen for convenience and its utility for demonstrating sidelobe recovery. The relationship between the spectrum of the aperture function and the test signal is illustrated in Fig. 5. The rectangular aperture for this study was chosen so that the first side lobe of the aperture is inside the spectrum of the test signal as illustrated in Fig. 5, allowing the reconstruction of the attenuated and nulled frequencies within the side lobe to be easily evaluated. Both noise-free and noisy cases are considered. For the noisy case multiplicative noise is added to the test signal a_{orig} using

$$a_{\text{noisy}} = (1 + 0.05N(0,1))a_{\text{orig}} \tag{5}$$

where $N(0,1)$ is a zero mean Gaussian random variable. This is a simplified version of the noise model for the ERS-1 scatterometer. It should be noted here that the scatterometer has different noise model than is usually used for a measurement system. Typical models use additive noise and the noise is usually independent of the measurement. With the scatterometer noise model, however, the noise is multiplicative and depends on the actual measurement value, further complicating the noise effects in the reconstruction algorithm.

To illustrate the resolution enhancement capabilities of the algorithms, we present a comparison of algorithm results for the noiseless measurement case. Since the algorithms can only be run a finite number of times, we also examine performance as a function of iterations. Figure 6 is comparison of the output of the three algorithms at 25, 100 and 1000 iterations with no noise. There are two significant observations to be made. First, there is little

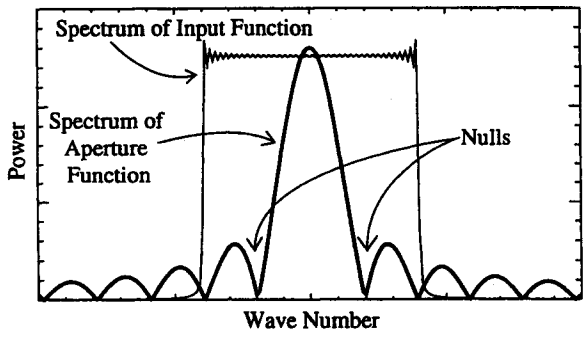

Figure 5. Illustration of the overlay of the test signal spectrum (light) with the frequency response of the aperture function (bold).

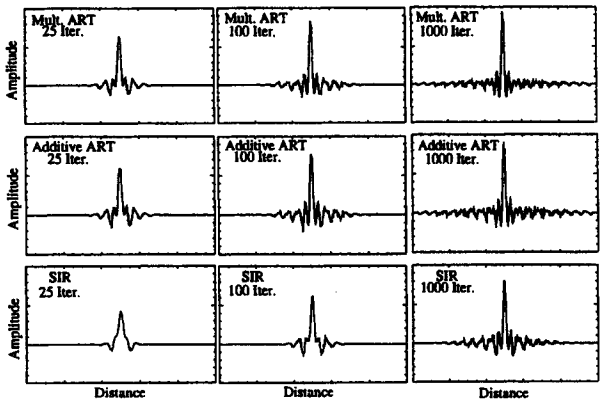

Figure 6. A comparison of SIR, additive ART and multiplicative ART outputs after 25, 100 and 1000 iterations for noiseless measurements. There is little difference between additive ART and multiplicative ART. SIR lags behind the the other two methods as a result of the non-linear damping designed to reduce the influence of noise on the output.

difference between the Additive ART and Multiplicative ART reconstructions. While there are some small numerical differences as would be expected from the use of two different algorithms, the differences are negligible.

Second, the SIR output lags (as a function of the number of iterations) the output of the other algorithms. In fact, the SIR output at 100 iterations and the output of Multiplicative and Additive ART at 25 iterations compare very well. This lag is a result of the bounded multiplicative scale factor used in the SIR algorithm. As is illustrated later, the bounded scale factor results in much better performance in the presence of noise.

Figure 7 shows the frequency domain representation of the output for 1000 iterations of all three algorithms. The important thing to note here is the behavior of the side lobes within the desired frequency band. Refer back to Fig. 5 and note that the aperture function has very low side lobes within the test signal frequency band. After processing, the side lobes within the test signal frequency band are essentially recovered. All three algorithms successfully reconstruct the original signal within the limits of the nulls in the aperture function as expected by the earlier theoretical development for the noiseless case. In previous work, an inverse filter to compensate for the lower side lobes resulting from incomplete reconstruction for SIR has been used with success.[4]

Figure 8 illustrates the spectra of the output from Multiplicative ART and SIR at 25 and 100 iterations for both noiseless and noisy cases. (Both additive and multiplicative ART produce similar results for these cases.) While the noiseless case shows very good spectral recovery for just a few iterations, the performance of the ART algorithms in the presence of noise is significantly degraded. After 100 iterations the energy in the noise outside the desired band is increasing rapidly for the ART algorithm.

The poor performance of ART in the presence of noise originally motivated the development of SIR.[11] For SIR,

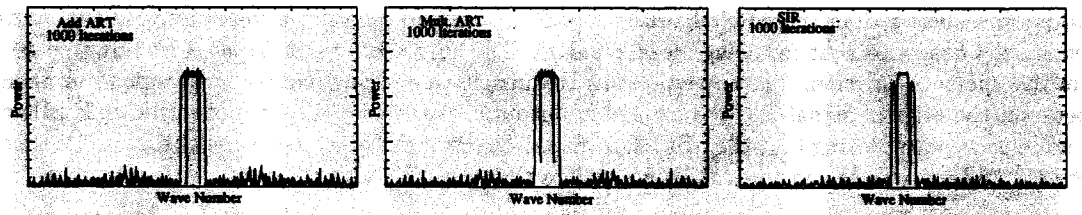

Figure 7. A frequency domain comparison of the outputs of SIR, additive ART, and multiplicative ART after 1000 iterations in the noiseless case. Note how all three examples show significant improvement of the side lobe levels compared with the original levels in Figure 5. After additional iterations SIR results are identical to the ART results.

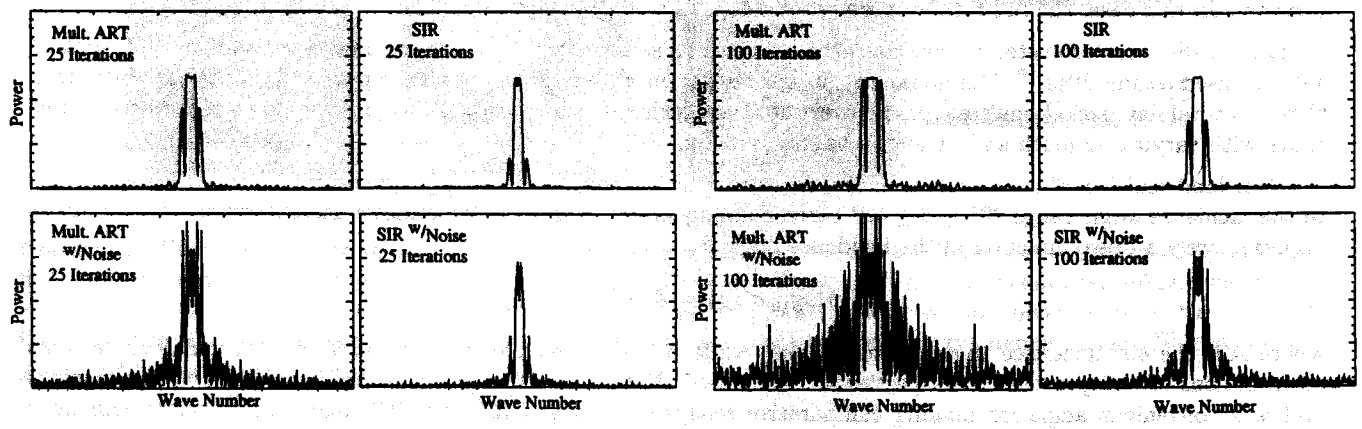

Figure 8. Spectra of multiplicative ART and SIR with noiseless and noisy measurements in the simulation.

the multiplicative scale factor is damped so that large scale factors do not overly magnify the noise at any one iteration, slowing the reconstruction but minimizing the effects of the noise. This is evident in the first sidelobe of the SIR estimate which, while enhanced, is not as noisy as it is for ART.

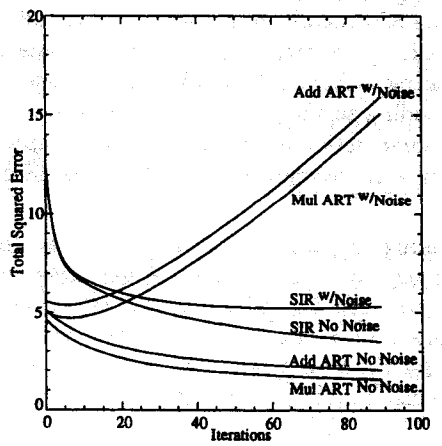

Figure 9. Cumulative squared error between the output of the algorithms for various iterations and noise.

Figure 9 compares the error performance of the three algorithms in the simulation. To compute the total squared error shown, the output at each iteration is subtracted from the original test function and the difference squared and summed. The noisy cases for multiplicative and additive ART show greater error with increasing iterations after a brief initial decrease. Even though the total squared error is low in the initial iterations for the ART algorithms, a minimum number of iterations (about 30) is required to generate acceptable resolution enhancement, in which case

SIR begins to perform better than the ART algorithms. SIR is also convergent to a lower total error than the ART algorithms which are nonconvergent for noisy measurements. The curves in Fig. 9 do not converge to zero because of the nulls in the aperture function. The corresponding frequencies are unrecoverable and result in some minimum error level between the original signal and the algorithm outputs. Based on Fig. 9 we conclude that SIR performs better when noise is present. Noting that the SIR algorithm also recovers the incidence angle response,[11] we conclude that it is better suited for application to scatterometer data than an ART algorithm.

5. APPLICATION TO ERS-1 SCATTEROMETER MEASUREMENTS

The original SIR algorithm was developed for the Seasat scatterometer where the aperture function could be approximated by a rect function, simplifying the algorithm.[11] The ERS-1 scatterometer aperture function is a cosine on a pedestal. In this case, the full response function is used in the SIR algorithm.[10]

Each ERS-1 scatterometer σ^o measurement consists of a series of pulses which are integrated and spatially filtered with a raised cosine filter.[10] The nominally 50 km resolution σ^o measurements are reported on a 25 km swath grid. Over a several day period, multiple passes over the study region can be collected with a given point observed multiple times with varying azimuth and incidence angles (see Fig. 10).

Over land and ice σ^o is a function of the measurement incidence angle, θ, and geophysical properties of the ice. In the incidence angle range $20° \leq \theta \leq 60°$ corresponding to the range of scatterometer measurements, σ^o (in dB) is approximately a linear function of the incidence angle θ

$$10 \log_{10} \sigma^o(\theta) = \mathcal{A} + \mathcal{B}(\theta - 40°) \tag{6}$$

where $\mathcal{A}$ is the 40° incidence angle-normalized σ^o, while $\mathcal{B}$ is the dependence of σ^o on θ. The $\mathcal{A}$ and $\mathcal{B}$ coefficients are functions of the geophysical properties of the surface. Note that 40° represents the mean θ of the observations and is a convenient angle for making comparative analyses. Unlike ART, the SIR algorithm provides enhanced resolution images of both $\mathcal{A}$ and $\mathcal{B}$ from multiple pass data. Combining multiple passes reduces the radiometric noise and permits estimation of the incidence angle response. Multiple passes require, however, the assumption that the surface is constant during the imaging time interval (see the discussion in Ref. 11).

To illustrate the application of SIR to ERS-1 scatterometer measurements, simulation is used. The geometry and response function from actual ERS-1 measurements over a small study region in Antarctica are used with synthetic $\mathcal{A}$ and $\mathcal{B}$ images (see Fig. 10) to generate simulated σ^o measurements. Monte Carlo noise is added to the measurements. The result of applying the SIR algorithm is shown in Fig. 10. The pixel resolution used is 8.9 km. For comparison, a nonenhanced $\mathcal{A}$ image is also shown. This image was generated from one pass by first incidence angle correcting the σ^o measurements using a fixed (-0.15 dB/deg) $\mathcal{B}$ value. Each pixel in the swath is assigned the resulting estimated $\mathcal{A}$ value corresponding to the measurement with the largest response for that pixel. While the SIR image uses all available σ^o measurements, only measurements from a single antenna beam can be used in the nonenhanced image. Though there is some overshoot, the SIR image effectively enhances the resolution of the resulting imagery.

While it is possible to use inverse filtering on the nonenhanced image to improve the effective resolution, the SIR algorithm provides an effective methodology to combine multiple antennas and passes to infer both the incidence angle normalized σ^o ($\mathcal{A}$) and the incidence angle dependence of σ^o ($\mathcal{B}$). Because SIR can infer the incidence angle response we conclude that it is better suited for application to scatterometer data than an ART algorithm. Because of the non-overlapping σ^o measurements for the Seasat and NSCAT scatterometer, multiple passes must be combined to achieve full surface coverage for these instruments, requiring the use of SIR.

6. SUMMARY

In this paper, we have presented the theory behind scatterometer resolution enhancement. Gröchenig's algorithm to recover an image from irregular samples was discussed. This algorithm is equivalent to additive ART. Experimental data was used to compare the reconstructive abilities of additive ART, multiplicative ART and SIR for both noise free and noisy cases. SIR performs substantially better in the presence of noise than comparable ART algorithms. The application of SIR to ERS-1 scatterometer measurements is illustrated with simulation. We conclude that SIR is an effective tool for scatterometer resolution enhancement.

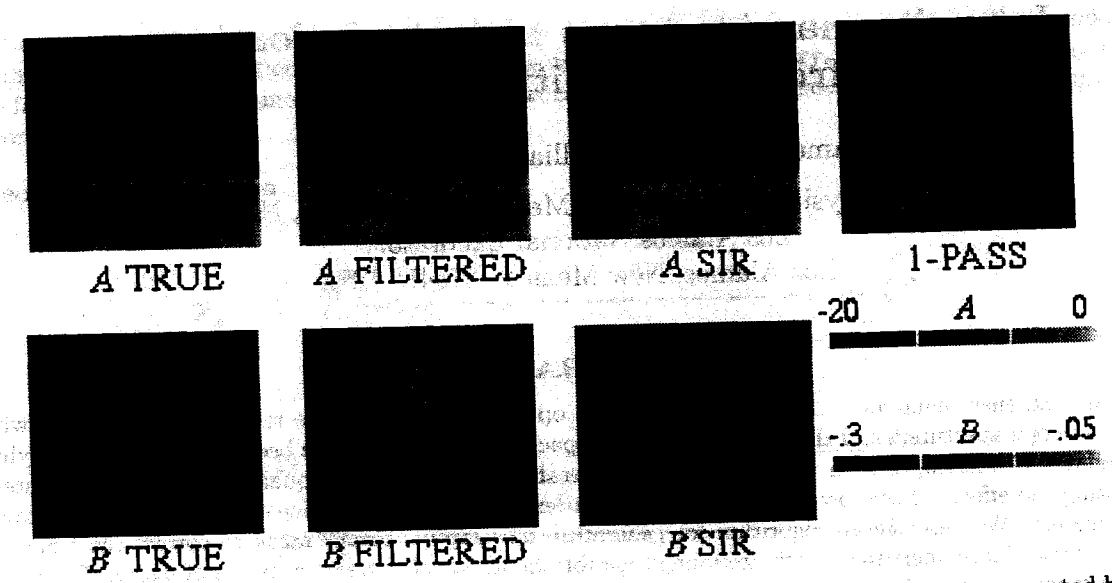

Figure 10. ERS-1 simulation results. The pixel resolution is 8.9 km. The filtered images were generated by lowpass filtering the original true images to 25 km resolution. These represent the best the resolution enhancement can achieve given the sampling. The nonenhanced 1-pass image was generated by setting pixel value to the value of the measurement covering the pixel with the largest gain. An incidence angle dependence image (B) can not be generated for the 1-pass case.

REFERENCES

1. E.P. Attema, "The Active Microwave Instrument On-Board the ERS-1 Satellite," *Proc. IEEE*, Vol. 79, No. 6, pp. 791-799, 1991.
2. K. Gröchenig, "Reconstruction Algorithms in Irregular Sampling," *Mathematics of Computation*, vol. 59, no. 199, pp. 181–194, 1992.
3. Y. Censor, "Finite series-expansion reconstruction methods," *Proc. IEEE*, vol. 71, no. 3, pp. 409–419, March 1983.
4. D. Daum, D. Long, and W. Davis, "Reconstructing Enhanced Resolution Images From Spaceborne Microwave Sensors," *Proc. IGARSS*, Pasadena, California, 8-12 August, pp. 2231–2233, 1994.
5. M. Drinkwater, D. Long, and D. Early, "Enhanced Resolution ERS-1 Scatterometer Imaging of Southern Ocean Sea Ice", *ESA Journal*, vol. 17, pp. 307–322, 1993.
6. D.S. Early and D.G. Long, "Enhanced Resolution Imaging from Irregular Samples," Submitted to, *IEEE Trans. Geosc. Remote Sens.*, 1997.
7. D. S. Early and D. G. Long, "Error and Resolution Characteristics of the SIRF Resolution Enhancement Algorithm," *Proc. IGARSS*, Lincoln, Nebraska, 27-31 May, pp. 124–126, 1996.
8. T. Elfving, "On Some Methods for Entropy Maximization and Matrix Scaling," *Linear Algebra and its Applications*, no. 34, pp. 321–339, 1980.
9. A. K. Jain, *Fundamentals of Digital Image Processing*, Prentice Hall, Englewood Cliffs, NJ, 1989.
10. D. Long, D. Early, and M.R. Drinkwater, "Enhanced Resolution ERS-1 Scatterometer Imaging of Southern Hemisphere Polar Ice," *Proc. IGARSS*, Pasadena, California, 8-12 August, pp. 156–158, 1994.
11. D. Long, P. Hardin, and P. Whiting, "Resolution Enhancement of Spaceborne Scatterometer Data," *IEEE Trans. Geosci. Remote Sens.*, vol. 31, pp. 700–715, 1993.